24th COBEM - 2017

24th ABCM International Congress of Mechanical Engineering
December 3-8, 2017, Curitiba, PR, Brazil

# COBEM-2017-2215
# DEVELOPMENT OF A CLIMBING ROBOT WITH MAGNETIC WHEELS

**Orlando Silva de Lima Junior**
**Marcelle Betzler Michels**
**Paulo Modesto Cordeiro da Silva**
CEFET-RJ, Undergraduate students of Control and Automation Engineering, Rio de Janeiro, Brazil
{orlandolimajnr, mbetzlerm, pmpaulomodesto}@gmail.com

**Fabrício Lopes e Silva**
**Cristiano de Souza de Carvalho**
**Luciano Santos Constantin Raptopoulos**
NUPEM/CEFET-RJ - Mechatronics Research Center of the Federal Center for Technological Education Celso Suckow da Fonseca, Rio de Janeiro, Brasil
{fabricio.silva, cristiano.carvalho, luciano.raptopoulos}@cefet-rj.br

***Abstract.*** *In this work is presented the study for the design of a robot that can climb ferromagnetic surfaces, which can be applied in inspections and maintenance tasks on vessels and similar structures. The proposed design uses for the adherence of the wheels to the surface and array of rare-earth magnets and steel wheels, arranged in two modules, each containing two wheels driven by an electric motor. To power this motor, a power board was designed together with a control board to make proper movement of the robot. In this work, studies were developed on the kinematics and dynamics of the mobile vehicle, the configuration adopted for the locomotion system and the surface adhesion. Afterwards, experiments were realized to evaluate the adhesion force for the designed wheel. As results of the work, an economical and feasible device for the locomotion on ferromagnetic surfaces was developed in a way that construction of this device is viable. Knowledge on this subject was established at CEFET-RJ, Nova Iguaçu campus.*

***Keywords:*** *magnetic, wheels, ferromagnetic, climbing, robot.*

## 1. INTRODUCTION

Inspections, painting and welding on metal surfaces are tasks that pose many risks to humans, including exposure to chemical compounds harmful to health and the possibility of falling from the structures. The use of an autonomous or even radio controlled system to perform these activities avoids the exposure of humans to dangerous situations, reduces expenses and increases the reliability of inspections, diagnostics, and solutions of possible problems in metal structures (Tavakoli *et al.*, 2013). The use of magnetic adhesion method on metallic surfaces is an important alternative used in the industry having a high level of reliability and low cost relative to other options, such as robots with adhesion systems based on vacuum suction, tapes with glue or claws. The need to create the own electronic prototyping platform is identified in the search for the ideal control for the locomotion of the robot.

## 2. ROBOT HARDWARE

Some experiments, simulations and projects were carried out using different software in order to form sufficient material for the construction of a climbing robot. The analyzes were carried out with care in order to make the project more economically feasible, bringing the maximum possible benefits to the interested parties.

### 2.1 Magnetic wheels

The wheel chosen for the design has a polypropylene base that functions as a carrier for the N35 grid neodymium magnets and two SAE 1010 steel rings that will be coupled to the sides of the polypropylene carrier so that the magnetic flux can be transmitted to the surface contact.

The proposed wheel was designed in a 3D CAD software and exported to ANSYS Maxwell® (Guide, 2015) to analyze how the number of magnets, width of the steel parts, and a layer of rubber could affect the magnetic force. As can be seen in Figure 1, the flux is contained on the ferromagnetic parts only.

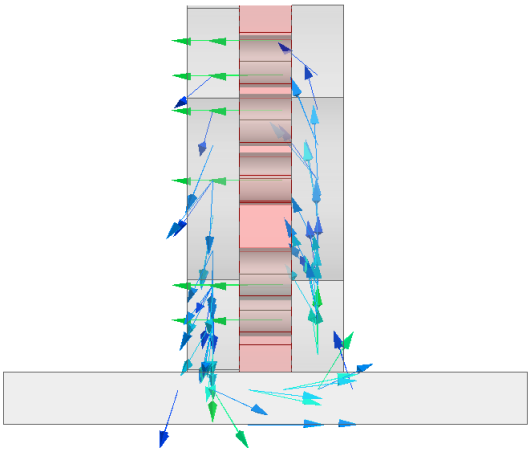

Figure 1. Designed wheel and its magnetic flux.

It's observed in the Table 1 the results of the simulations when varying the number of magnets on the wheel configuration. Increasing the number of magnets would also increase the magnetic force, almost in a linear way. Therefore, the addition of magnets is a solution to obtain a higher magnetic force, as expected.

Table 1. Variation of the magnetic force due to addition of magnets.

| Number of magnets | Magnetic force (Newtons) |
|---|---|
| 5 | 153.760 |
| 6 | 178.930 |
| 7 | 217.010 |
| 8 | 234.490 |
| 9 | 253.630 |
| 10 | 292.030 |

In Table 2, the results of the magnetic force simulation are given as a function of the variation of the width of the steel rings used on the sides of the wheel. It is observed that the magnetic force increases proportionally to the width of the rings. Thus, through a combination of magnets and steel rings, the proposed wheel can meet design specifications. Finally, a layer of rubber was added to the design and the magnetic force was simulated. With a 2 mm thick layer, taking into account the configuration with 5 magnets and steel rings 10 mm wide, the strength was reduced from 153.760 N to 39.391 N. The performance of the magnetic adhesion decreased significantly, making the rubber layer unsuitable for some applications.

Table 2. Variation of the magnetic force due to increasing of steel ring's width.

| Width of the steel ring (mm) | Magnetic force (Newtons) |
|---|---|
| 5 | 153.760 |
| 7.5 | 178.930 |
| 10 | 217.010 |
| 12.5 | 234.490 |
| 15 | 253.630 |

For the purposes of this work it was assumed that the mobile robot must have a payload of 20 kg and taking this into consideration in conjunction with the results of the simulations presented the following configuration of wheels for the project: 5 magnets, 10 mm thick steel disc and no use of rubber coating. A wheel model was designed using two steel rings of 69 mm of external diameter, 35 mm of internal diameter and 10 mm of thickness. The polypropylene base is 65 mm in diameter and 30 mm thick (Fig. 2.).

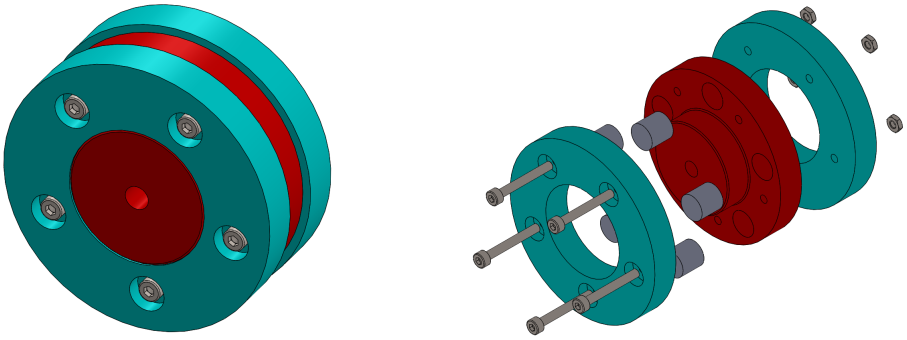

(a) (b)

Figure 2. Proposed wheel: (a) Assembled wheel, (b) Exploded view.

The interaction of this wheel with a steel surface of SAE 1020 was simulated to verify the magnetic force and how the magnetic flux behaves in this configuration. Figure 3 represents the distribution of the magnetic flux density on the proposed wheel. This simulation shows that the stainless-steel screws used to assemble the parts of the wheel do not provide a path for the magnetic flux, which avoids a reduction on the total magnetic force, maintaining the grip of the wheel.

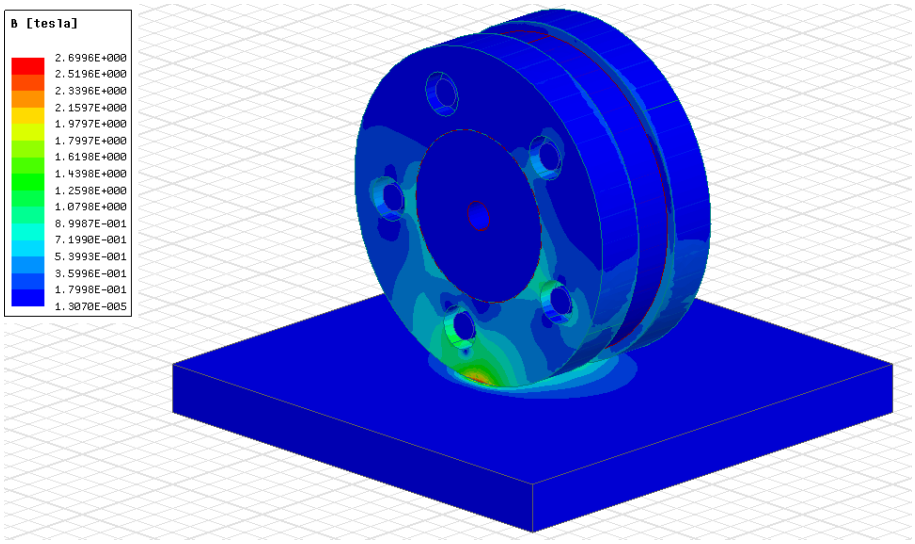


Figure 3. Analysis of magnetic flux density.

## 2.2 Morfology

The arrangement of the wheel will be unicycle, that is two wheels reduced in one. Will therefore have a right and left module to make the robot move. As a pair of wheels will be used in each one it was decided to check how it would interact with each other at certain distances. According to the simulation of the Figure 4 the left wheel has an attractive force of 88.929 N with the magnetic surface and only 0.394 N due to the contact with the other wheel. Due to the geometry chosen by the wheels, most of the magnetic flux passes through the surface and returns to the magnets without passing through the other wheel. With this, the two wheels can be placed side by side in the model without the aid of a barrier. Each module of the robot will have a payload of 10 kg, giving a total of 98.1 Newtons of payload per module.

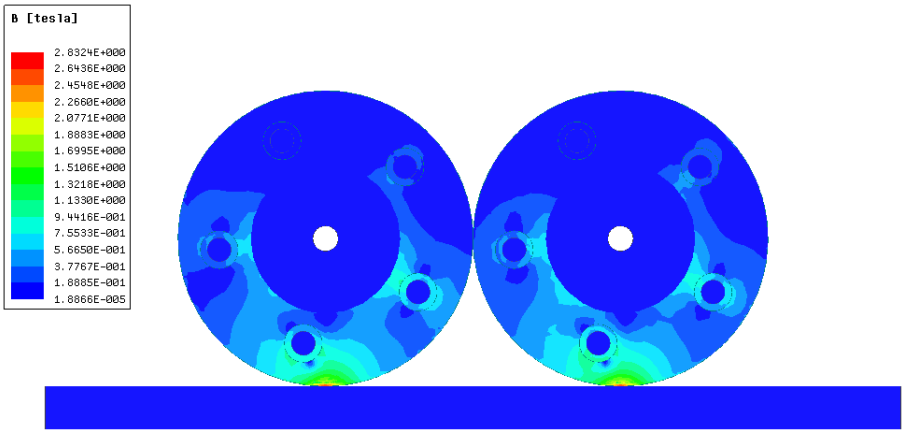


Figure 4. Distribution of the magnetic flux between two wheels.

### 2.3 Wheel traction

After the simulations, a wheel was built and experimental tests with a load cell were performed to compare the simulation results with the experimental tests. The surface used was a SAE 1020 steel disc of 63.5 mm in diameter and 16 mm in thickness. The mounted wheel on the load cell is demonstrated in the Fig. 5.

Figure 5. Experimental tests with a load cell.

After assembling the test surface and the wheel, it was placed in contact with the SAE 1020 steel disc to perform the tensile tests. After the wheel was drawn and the force realized for total uncoupling of the wheel to the surface. During the tests curves of the tensile force exerted until the decoupling of the wheel with the contact surface. In the Figure 6 is presented the graph for the test in which the complete wheel was lifted from the surface to a speed of 100 mm / minute.

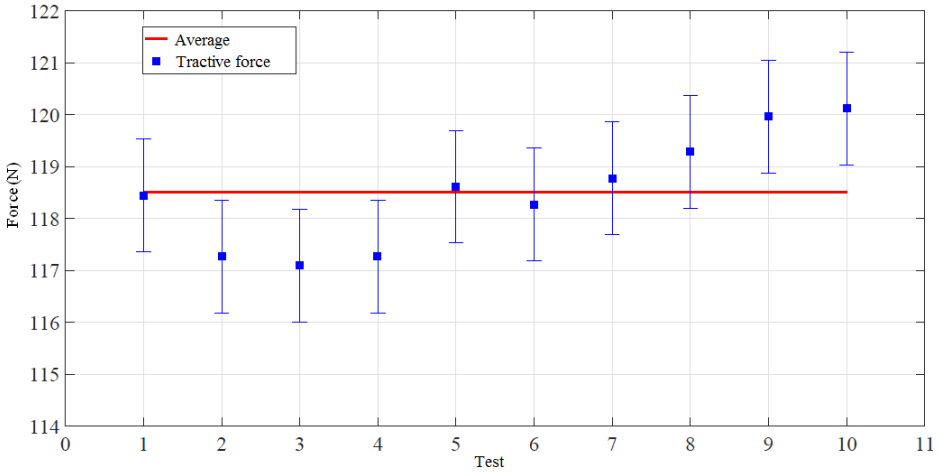


Figure 6. Variation of the traction force for experiments performed with velocity of 100 mm / min for lifting the complete wheel.

Comparing the results of the experiments of this type of test with the results of the simulations, it can be seen that the values are close. The average for this set of tests was 118,506 N, whereas, the simulation for this case resulted in 125,950 N. This equates to a difference of 5.910% between the values. The reason for the variation of the tensile force between the different types of test is the relative movement of the wheel when it is being raised to discover the maximum tensile force it supports before losing grip with the surface ferromagnetic.

### 2.4 Forward kinematics

The kinematics is the part of mechanics that studies the geometry of body movement without taking into account the forces, only position, orientation, velocity and accelerations (Siegwart *et al.*, 2011). For the kinect modeling of mobile robot, it is considered the same with rigid body on wheels operating on a horizontal plane. A reference is necessary to represent the vectors. This inertial reference system is presented by the axes $\overrightarrow{OX_R}$ e $\overrightarrow{OY_R}$. You must have a mobile reference to describe this robot. This system consists of the axes $\overrightarrow{QX}$ e $\overrightarrow{QY}$. The origin of this mobile system is chosen to be the reference point to describe the position (Tzafestas, 2013).

The kinematic analysis of the robot is presented so that it may be possible to understand how the position of the robot and the orientation vary with respect to the velocities of the wheels. In Figure 7 the geometry and the kinematic parameters of a robot with traction differential and a beaver wheel are presented:

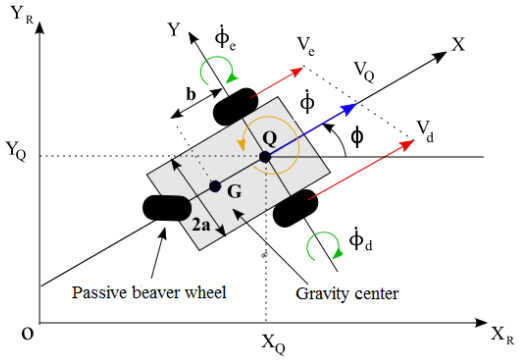


Figure 7. Geometry of a robot with differential traction.

It was assumed that the wheels rotate without slipping, the axis of rotation of the robot are perpendicular to the plane $OX_RY_R$ and the point Q coincides with the center of mass of the robot. The kinematic model of the robot was developed for analysis of the robot's behavior during it's movement and for possible use in the control law that can be applied to it.

$v_e$ e $v_d$ are the linear velocities of the left and right wheels, respectively, $v_Q$ is the velocity of the point Q and can be expressed by the following equations:

$$v_d = v_Q + a\dot{\phi}; \quad (1)$$

$$v_e = v_Q - a\dot{\phi}; \quad (2)$$

Adding and subtracting $v_d$ e $v_e$ gets:

$$v_Q = \frac{1}{2}(v_e + v_d); \quad (3)$$

$$2a\dot{\phi} = v_d - v_e; \quad (4)$$

and due to he non-slip hyphotesis, we have $v_d = r\dot{\phi}_d$ e $v_e = r\dot{\phi}_e$

$$\dot{X_Q} = v_Q cos(\phi); \quad (5)$$

$$\dot{Y_Q} = v_Q sen(\phi); \quad (6)$$

Kinematic model of the robot with differencial traction can be described by the equations:

$$\dot{x_Q} = \frac{r}{2}(\dot{\phi_d} cos\phi + \dot{\phi_e} cos\phi) \quad (7)$$

$$\dot{y_Q} = \frac{r}{2}(\dot{\phi_d} sin\phi + \dot{\phi_e} sin\phi) \tag{8}$$

$$\dot{\phi} = \frac{r}{2a}(\dot{\phi_d} - \dot{\phi_e}) \tag{9}$$

which can be rewritten as:

$$\dot{Q} = \begin{bmatrix} \frac{r}{2}cos(\phi) \\ \frac{r}{2}sen(\phi) \\ \frac{r}{2a} \end{bmatrix} \dot{\theta_d} + \begin{bmatrix} \frac{r}{2}cos(\phi) \\ \frac{r}{2}sen(\phi) \\ \frac{-r}{2a} \end{bmatrix} \dot{\theta_e} \tag{10}$$

or,

$$\dot{Q} = J\dot{q}; \tag{11}$$

where:

$$\dot{Q} = \begin{bmatrix} \dot{X} \\ \dot{Y} \\ \dot{\phi} \end{bmatrix} \tag{12}$$

$$\dot{q} = \begin{bmatrix} \dot{\theta_d} \\ \dot{\theta_e} \end{bmatrix} \tag{13}$$

being **J** the jacobian of the mobile robot is expressed by:

$$J = \begin{bmatrix} \frac{r}{2}cos(\phi) & \frac{r}{2}cos(\phi) \\ \frac{r}{2}sen(\phi) & \frac{r}{2}sen(\phi) \\ \frac{r}{2a} & \frac{-r}{2} \end{bmatrix} \tag{14}$$

Eliminating $v_Q$ of the equations 5 and 6 non-holonomic restriction is obtained:

$$-\dot{X}_Q sen(\phi) + \dot{Y}_Q cos(\phi) = 0 \tag{15}$$

which demonstrates that the point Q located in the mobile robot moves along the axis Qx and that it's velocity along the axis Qy is zero, that is, there is no lateral displacement.

The Jacobian matrix **J** has three rows and two columns, which means that it is not an invertible array. In this case the solution to the equation 14 is given by:

$$\dot{q} = J^{\dagger}\dot{Q} \tag{16}$$

$\mathbf{J}^{\dagger}$ can be computed from Eq. 1 and Eq. 2.

$$v_Q = \dot{X_Q} cos(\phi) + \dot{Y_Q} sen(\phi) \tag{17}$$

Replacing in equation 1 and 2 gets:

$$r\dot{\theta_d} = \dot{X_Q} cos(\phi) + \dot{Y_Q} sen(\phi) + a\dot{\phi} \tag{18}$$

$$r\dot{\theta_e} = \dot{X_Q} cos(\phi) + \dot{Y_Q} sen(\phi) - a\dot{\phi} \tag{19}$$

which can be rewritten as:

$$\begin{bmatrix} \dot{\theta_d} \\ \dot{\theta_e} \end{bmatrix} = \frac{1}{r} \begin{bmatrix} cos(\phi) & sen(\phi) & a \\ cos(\phi) & sen(\phi) & -a \end{bmatrix} \begin{bmatrix} \dot{X_Q} \\ \dot{Y_Q} \\ \dot{\phi} \end{bmatrix} \tag{20}$$

where:

$$J^{\dagger} = \frac{1}{r}\begin{bmatrix} cos(\phi) & sen(\phi) & a \\ cos(\phi) & sen(\phi) & -a \end{bmatrix} \tag{21}$$

The non-holonomic restriction can be rewritten as follows:

$$M\dot{p} = 0, \quad M = \begin{bmatrix} -sen(\phi) & cos(\phi) & 0 \end{bmatrix} \tag{22}$$

If $\dot{\phi}_d \neq \dot{\phi}_e$, the difference between $\dot{\phi}_d$ and $\dot{\phi}_e$ determines the rotation and speed of the robot as well as it's direction. The instanteneous radius of curvature **R** is given by:

$$R = \frac{v_Q}{\dot{\phi}} = a\frac{v_d + v_e}{v_d - v_e}, \quad v_d \geq v_e \tag{23}$$

and the instantaneous coefficient of curvature is:

$$k = \frac{1}{R} \tag{24}$$

### 2.5 Dynamic model

Dynamic analysis is important because it considers how the dynamic variables (for example: masses, system inertias and geometric parameters) affect the handling of the vehicle in question. The model presented here is based on in the Lagrangian formulation for the development of the dynamic equations. This one method is based on the Lagrangian definition which is:

$$L = K - P = L(q, \dot{q}) \tag{25}$$

where **K** is the total kinetic energy of the system and **P** is the total potential energy of the system. For this analysis was not considered the potential energy of the mobile robot however, it should be included later in future work. The position of the mobile robot can be defined without inertial reference system **O**XRYR by the position of the center of gravity of the theft asked by **G** or the position of the mid-point of the axle connecting as wheels with actuators, denoted by **Q**.

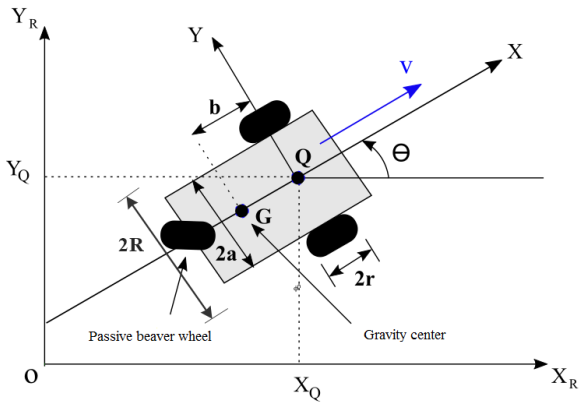


Figure 8. Dynamic model of the mobile robot.

The potential energy of the system was disregarded in this model due to the fact that that the magnetic forces are many greater than the weight strength of the robot, taking considering the payload of 20 kg. In this way it is concluded that the Lagrangian is only composed of the total kinetic energy of the system. The Lagrangian equations for this system are:

$$\frac{d}{dt}\left(\frac{\partial L}{\partial \dot{\theta}_{\mathrm{D}}}\right) - \frac{\partial L}{\partial \theta_D} = \tau_D \tag{26}$$

$$\frac{d}{dt}\left(\frac{\partial L}{\partial \dot{\theta}_{\mathrm{E}}}\right) - \frac{\partial L}{\partial \theta_{\mathrm{E}}} = \tau_E \tag{27}$$

where $\tau_E$ e $\tau_D$ are the torques of the left and right engines, respectively.

To dimension the electrical motor capacity necessary to rotate the wheels in the desired speed was used the dynamic model of the proposed robot, described in the following equations:

$$A\ddot{\theta}_D + B\ddot{\theta}_E = \tau_D \tag{28}$$

$$B\ddot{\theta}_D + A\ddot{\theta}_E = \tau_E \tag{29}$$

Where:

$$A = \frac{Mr^2}{4} + \frac{(I_Q + Mb^2)}{4R^2}r^2 + I_o \tag{30}$$

$$B = \frac{Mr^2}{4} - \frac{(I_Q + Mb^2)}{4R^2}r^2 \tag{31}$$

### 2.6 Planning of trajectory

This step is important for the locomotion of the robot to meet it's path in the workspace. There is a method (Costa *et al.*, 2008) of planning of trajectory that integrates the generation of the path that will be traveled and the kinematics and dynamics constraints of the mobile robot using polynomials of degree 5 to attend the restrictions. Through this method it is possible to analyze in a more comprehensive way the behavior of robot during the trajectory chosen.

The initial conditions for the trajectory of mobile robot were chosen:

- $X_i$ = 0. (x coordinate of the initial position)
- $Y_i$ = 0. (y coordinate of the initial position)
- $\theta_i$ = 0. (Orientation of robot at departure point)
- $v_i$ = 0. (Linear velocity of robot at departure point)
- $\omega_i$ = 0. (Angular velocity of robot at departure point)

then the final conditions:

- $X_f$ = 2. (x coordinate of the final position)
- $Y_f$ = 1. (y coordinate of the final position)
- $\theta_f = \frac{\pi}{3}$. (Orientation of robot at the target point)
- $v_f$ = 0. (Linear velocity of robot at point of arrival)
- $\omega_f$ = 0. (Angular velocity of robot at point of arrival)

For the analyzes a total time of 40 seconds was chosen for the robot to go from it's initial position to it's final position.

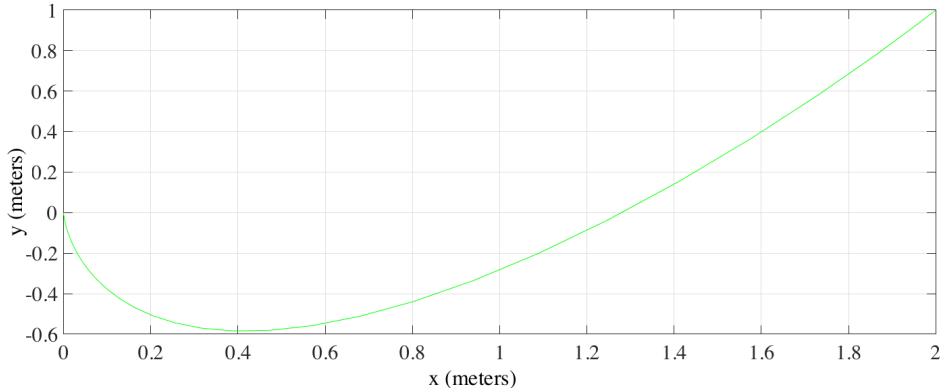


Figure 9. Trajectory generated by the robot.

With the results found, the torque of the wheels was verified through the dynamic model. The graph was produced in MATLAB® and as we can see in Fig. 10 there is little variation in the torque between the wheels because large torque is required to move them. The analysis of these results is essential for the sizing of the robot's motors.

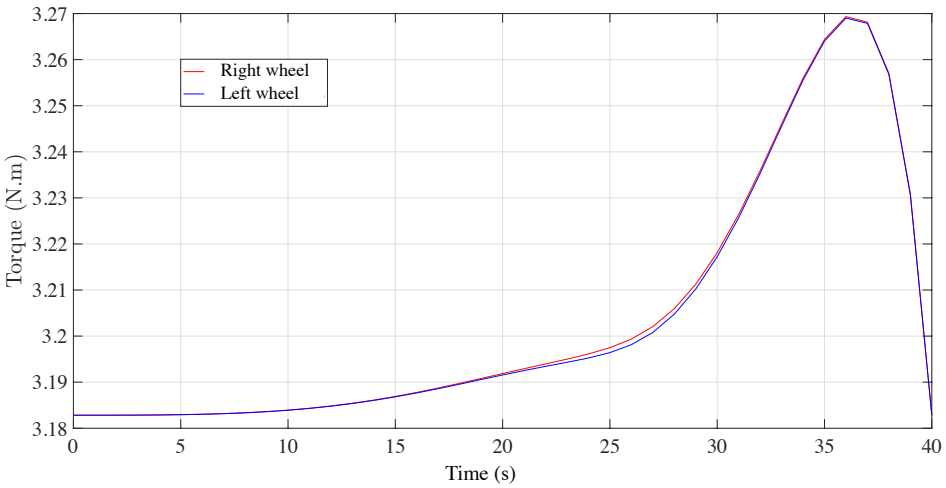


Figure 10. Variation of the torque of the left and right wheels during the trajectory of the mobile robot in the established time.

### 2.7 Electronic project

To support the mechanical study, the electronics were developed in an electronic design automation software for PCB (printed circuit board). As the robot contains two modules with magnetic wheels, so two motors are needed - one for each module - to provide sufficient torque for proper locomotion. A power board is needed, precisely because the electric current supplied at the micro-controller output is low. The two parts were built together, aiming for spatial and qualitative improvement. For the control part, voltage regulator circuits to 5 V via the LM 7805 and 3.3 V via the LM 1117. Both have voltage up to 20 V. The ECS-110-S-5P crystal, which operates at 16 MHz, was placed is an oscillator that presents enormous stability of frequency obtained. The indicator circuit has been created so that anyone able to program the board can be capable of receiving a feedback response from the microcontroller. They were arranged, therefore, six LEDs. The SN 75176 transceiver was chosen for communication in the RS-485 standard. This was the default choice, since the RS-232 allows only one transmitter and one receiver on each line, while it allows up to 32 devices to communicate through the same data line. It is important to note that the RS-485 standard is based on the differential transmission of data, through a pair of wires, which is ideal for long distances (reaches more than 1 km) in environments even though it is not immune to noise. A RESET button has been set if you want to restart or delete options (back to the default), as in the case of locking the microcontroller and the program stops working. By the way, for the choice of the microcontroller, we chose the ATMEGA 2560 16u (Fig. 11).

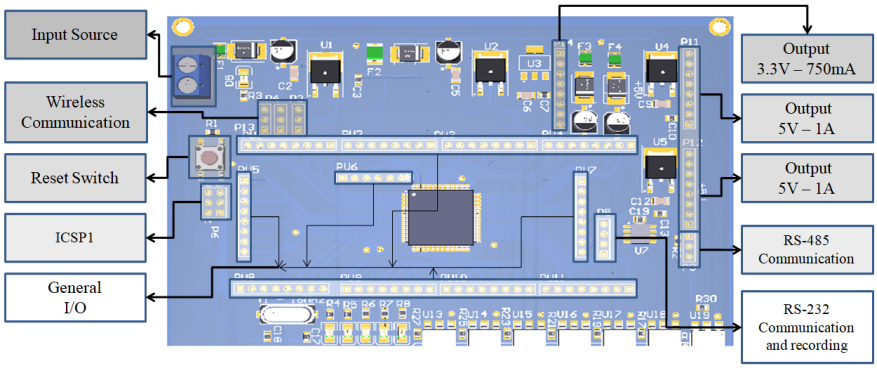


Figure 11. Description of the control part of the robot board.

With the results presented it was possible to verify the torque of the robot wheels according to the dynamic model. At least each engine must be capable of delivering a torque of 3.265 N.m that the robot leaves the starting point and reaches the end point at the predetermined time. Using a safety factor of 2 it is concluded that the motor shall be capable of delivering at least 6.530 N.m of torque for each wheel. The chosen motor is powered with 12 volts DC, consumption

of 1.3 A and 9.12 N.m of torque. Therefore, the power component BTS 7960 was chosen which is a half-bridge H that provides cost-optimized and low-cost solution, whose some of it's specifications can be seen in Tab. 3. To use it effectively are placed four of them, supplying the requirements of the engines. To use it effectively are placed four of them, supplying the requirements of the engines.

Table 3. Half-brige H data.

| Parameter | Value |
|---|---|
| PWM capacibility | up to 25 kHz |
| Consumption | 3 mA |
| Current | up to 43 A |
| Voltage | up to 45 V |

To maintain the output voltage of the electric circuit, was chosen TLE 4278. It's used because there is a voltage limitation for the microcontroller, so one input voltage between 5,5 V and 45 V is regulated to 5 V, causing no damages to this component. Somethings are important to have in this project, specially in this part, so the TLE 4278 has over temperature protection, short-circuit proof and wide temperature range. The temperature range is crucial for the type of places the robot can work. In order to maintain the correct polarity, the MOSFET SPD50P03L. It's a field effect transistor that amplify voltage. Electronic project needs protection and separation between the elements, with this purpose at the end of the power section of the board are optocouplers to perform the galvanic isolation, ensuring that the parts do not damage for example in the event of a short circuit.

Was awarded the 4N25 that has low power consumption. Each optocoupler consists of gallium arsenide infrared LED and a silicon NPN phototransistor. When the LEDs turns on, the phototransistor saturates leading to what is connected to it. It uses the light emitted to transmit signal from one circuit to another, avoiding and electrical connection between who sends and who receives. The contribution of this model is due to it's high switching speed, low current consumption, total insulation and the fact that it does not have mechanical parts. All this command components are illustrated in the Fig. 12.

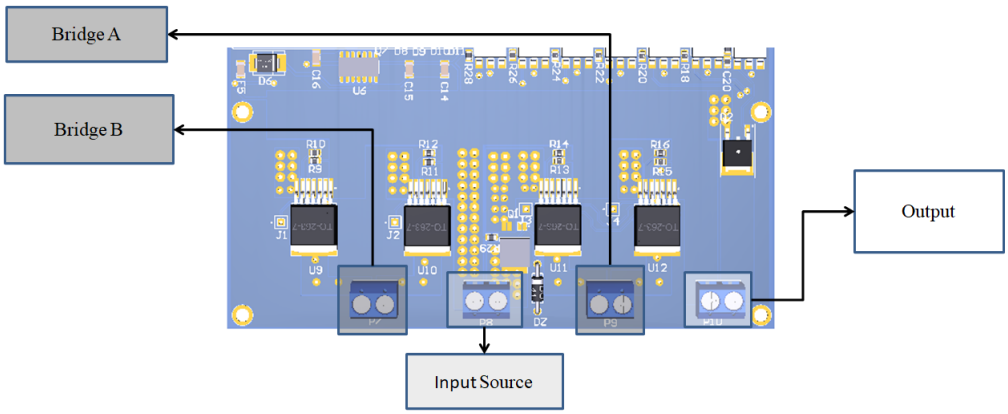


Figure 12. Description of the power part of the robot board.

This board is designed to meet the electrical requirements of this robot and provide support for possible upgrades and insertion of new inspection (Schmidt and Berns, 2013) instruments and various sensors. In addition to providing two modes of communication: wireless that allows the robot a great mobility and the other by wire being very resistant to electromagnetic interference (RS-485). It has the advantage of counting internally with the drives that supply high current (35 A) for powering the motors. In the Figure 13 is illustrated the electronic model already with its 3D components, where the top is the one that commands the robot and the bottom that controls the engines. Economically attractive options were chosen.

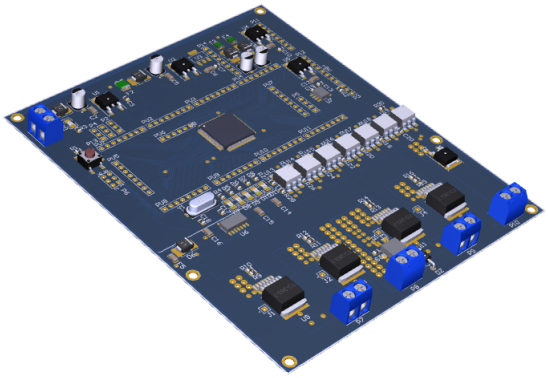

Figure 13. PCB Project with dimensions 122 x 146 mm.

## 3. ACKNOWLEDGEMENTS

This work was partially supported by COLAT/DIPPG/CEFET-RJ.

## 4. CONCLUSIONS

This study provided the analysis of the validity of the development of the robot with magnetic wheels. As discussed, the difference between the simulation and the experimental tests is very small, which confirms the prediction of the magnetic force according to the finite element analysis software. The difference between the experimental results and the simulations was 5.910%, which is very satisfactory in engineering development.

It was also possible to verify the feasibility and reliability of the construction of magnetic wheels. According to the experimental results and the simulations, the proposed magnetic wheel meets the requirements of the design, and has more force than is necessary for the ferromagnetic surfaces of the robot without risk of losing contact with them.

The electronic circuit is completely effective and covers all project objectives. In addition to leaving space for future work in various applications, it can be used with motors that consume up to 43 A. The size of the plate was adequate to contemplate sufficient channels of entry and exit, and can be used in large projects beyond the proposed, opening the possibility of sending various types of sensors to the vehicle.

## 5. REFERENCES

Costa, T.A.A., Ferreira, A.M. and Dutra, M.S., 2008. "Parametric trajectory generation for mobile robots". In *ABCM Symposium Series in Mechatronics*. Vol. 3, pp. 300–307.

Guide, A.U., 2015. "Maxwell 3d simulation".

Schmidt, D. and Berns, K., 2013. "Climbing robots for maintenance and inspections of vertical structures—a survey of design aspects and technologies". *Robotics and Autonomous Systems*, Vol. 61, No. 12, pp. 1288–1305.

Siegwart, R., Nourbakhsh, I.R. and Scaramuzza, D., 2011. *Introduction to autonomous mobile robots*. MIT press.

Tavakoli, M., Viegas, C., Marques, L., Pires, J.N. and De Almeida, A.T., 2013. "Omniclimbers: Omni-directional magnetic wheeled climbing robots for inspection of ferromagnetic structures". *Robotics and Autonomous Systems*, Vol. 61, No. 9, pp. 997–1007.

Tzafestas, S.G., 2013. *Introduction to mobile robot control*. Elsevier.

## 6. RESPONSABILITY NOTICE

The authors are the only responsible for the printed material included in this paper.